Available online at www.sciencedirect.com
SCIENCE DIRECT®
Journal of Molecular Catalysis A: Chemical 225 (2005) 259–269
JOURNAL OF MOLECULAR CATALYSIS A: CHEMICAL
www.elsevier.com/locate/molcata

Role of Pt-precursor on the performance of $Pt/BaCO_3/Al_2O_3{\cdot}NO_x$ storage catalysts

Jazaer Dawody[a,b,*], Magnus Skoglundh[a,c], Staffan Wall[d], Erik Fridell[a,b]

[a] *Competence Centre for Catalysis, Chalmers University of Technology, SE-41296 Göteborg, Sweden*
[b] *Department of Applied Physics, Chalmers University of Technology, SE-41296 Göteborg, Sweden*
[c] *Department of Materials and Surface Chemistry, Chalmers University of Technology, SE-41296 Göteborg, Sweden*
[d] *Department of Physical Chemistry, Göteborg University, SE-41296 Göteborg, Sweden*

Received 9 July 2004; accepted 1 September 2004

Abstract

The influence of the choice of platinum precursor on the catalytic performance of $Pt/BaCO_3/Al_2O_3$ NO_x storage catalysts was studied. The precursors used in the preparation of the catalysts were: (i) hexachloroplatinic acid $[H_2Pt(Cl)_6]$, (ii) tetraammineplatinum hydroxide $[Pt(NH_3)_4(OH)_2]$, (iii) diammineplatinum nitrite $[Pt(NH_3)_2(NO_2)_2]$ and (iv) platinum nitrate $[Pt(NO_3)_2]$. The catalytic activity of the prepared catalysts was tested for continuous lean NO_x reduction with C_3H_6, NO_x storage and reduction, and NO_2 dissociation in a flow reactor. The reactor experiments show that the sample prepared using platinum nitrate is the most active catalyst followed by the catalyst prepared from tetraammineplatinum hydroxide. The catalyst prepared from hexachloroplatinic acid is more active for continuous NO_x reduction, and NO_x storage and reduction than the catalyst prepared from diammineplatinum nitrite, but deactivates faster during NO_2 dissociation than the catalyst prepared using diammineplatinum nitrite.

In order to be able to predict mechanisms for the interaction between the platinum precursors and the $BaCO_3/Al_2O_3$ surface during the platinum impregnation, powder samples of γ-Al_2O_3, $BaCO_3$ and $BaCO_3$ precipitated on γ-Al_2O_3 were studied using FTIR and zeta potential measurements. Additionally, XRD measurements were performed to verify the transformation of the barium precursor to $BaCO_3$. The results from these studies show that up to 18% BaO content, the $BaCO_3/Al_2O_3$ surfaces contain domains of both $BaCO_3$ and Al_2O_3.

Keywords: Pt precursors; NO_x storage; Zeta potential; FTIR; $BaCO_3$

1. Introduction

Combustion engines contribute significantly to the consumption of fuel and consequently also to the anthropogenic emissions of CO_2. Increasing awareness of climate change and the connection between accumulated CO_2 in the atmosphere and global warming [1] emphasizes the need to reduce vehicle fuel consumption. Fuel economy can be improved by increasing the air-to-fuel ratio, i.e. to run the engine lean. However, the high concentration of oxygen in lean-burn engines gives rise to a drastic increase in NO_x ($NO + NO_2$) emissions, since in these conditions the reducing agents in the exhaust gas are more favorably oxidized by oxygen than NO_x in conventional catalytic converters for cars.

The so-called NO_x storage technology solves this problem by adding a NO_x storage component to the catalyst to store NO_x as nitrates during lean conditions until the catalyst becomes saturated. Thereafter, the catalyst is exposed to a net-reducing exhaust composition for a short time to decompose and reduce the stored nitrate to N_2 whereby the storage sites become regenerated [2–4].

A typical NO_x storage catalyst consists mainly of a high surface area metal oxide such as alumina, a NO_x storage component (often BaO or $BaCO_3$) and precious metals such as Pt or Pd and Rh. NO_x storage catalysts work satisfactorily

* Corresponding author. Tel.: +46 31 7724541; fax: +46 31 7723134.
E-mail address: jazaer.dawody@fy.chalmers.se (J. Dawody).

1381-1169/$ – see front matter © 2004 Elsevier B.V. All rights reserved.
doi:10.1016/j.molcata.2004.09.011

for sulphur-free fuels. The presence of sulphur in the fuel poisons the catalyst due to the formation of thermally stable sulfates with the storage material [5–10] and the decrease in the reduction capacity of the precious metal due to the accumulation of sulphur species on the noble metal during net-reducing conditions [9].

The research on NO_x storage technology has provided quite good understanding of the NO_x storage and sulphur poisoning mechanisms. However, it is not clearly known how to avoid the sulphur poisoning, improve the temperature stability and enhance the NO_x storage capacity. Further research thus is required to solve these limitations. One interesting issue in this respect is to study the interactions between the precious metals, the storage component and the support material, since some studies have shown that the spill-over of NO_x from or to Pt is important for efficient storage and reduction [4,6,11,12]. Interesting information can be obtained by investigating the processes that take place during the catalyst preparation.

For Pt/Al_2O_3 catalysts, processes such as Pt–alumina interaction, Pt complex decomposition during drying and calcination, and washcoating have been studied by many researchers [13–23]. The outcome of these studies is of great importance for the interpretation of the performance of catalysts based on Pt/Al_2O_3. However, additional studies are of interest when a storage component is added to the Pt/Al_2O_3 catalyst, since the storage material, e.g. BaO, modifies the Al_2O_3 surface, which may affect the interaction between Pt and the support material.

For Pt/Al_2O_3 attention has been given to the effect of both the type of Pt precursor and the pH during impregnation on the Pt dispersion. For this reason different types of alumina support materials and Pt precursors have been investigated. In some of these works, zeta potential measurements have been used to study the surface charge of alumina as a function of pH [14,20,23,24]. In general, these studies show that the alumina surface is positively charged at $pH < 8$, zero charged at pH 8–9 and negatively charged at $pH > 9$. This means that negatively charged Pt species adsorb on alumina at $pH < 8$ and positively charged Pt species adsorb on alumina at $pH > 9$ due to electrostatic interaction.

The chemical properties of the precious metal precursor used in the catalyst preparation play an important role in the interaction of the precious metal with the surface. This interaction influences the precious metal particle size and distribution on the surface. Thus, knowledge concerning chemical properties and stability of the precious metal precursor is important for the catalyst preparation processes. Among the Pt-precursors used in this study, most information is found in the literature on hexachloroplatinic acid, particularly; data on hydrolysis, speciation and stability [13,16,17,25].

In this work, we have studied the effect of the type of Pt precursor on the activity for continuous NO_x reduction, NO_x storage and NO_2 dissociation of $Pt/BaCO_3/Al_2O_3$ catalysts. The selection of the Pt-precursors was in accordance with the principle of surface polarization of the support materials upon impregnation with acidic or basic Pt-precursor solutions [14]. Since the removal of chlorine traces after impregnation with chlorine containing Pt-precursors is demanding, both chlorine containing and chlorine-free Pt-precursors were included in the study. The ammine complexes were also of interest due to the basicity of these solutions, and also since they are widely used in many types of catalysts. Accordingly, the following Pt precursors were used in the impregnation of the $BaCO_3$ and Al_2O_3 washcoated monoliths: hexachloroplatinic acid, platinum nitrate, tetraammineplatinum hydroxide and diammineplatinum nitrate. The impregnation using the first two precursor solutions was performed under acidic conditions, while the impregnation using the last two ones was performed under basic conditions.

In order to study the surface properties of $BaCO_3/Al_2O_3$, we precipitated $BaCO_3$ on γ-alumina and performed FTIR and zeta potential measurements to compare the surface properties of this sample with pure $BaCO_3$ and Al_2O_3 samples.

2. Experimental

2.1. Sample preparation

2.1.1. Powder samples for zeta potential and FTIR measurements

Zeta potential and FTIR measurements were performed using powder samples of γ-Al_2O_3 (SBa-200) from SASOL, $BaCO_3$ (99.99%) from Sigma-Aldrich and $BaCO_3$ precipitated on γ-Al_2O_3. The $BaCO_3/Al_2O_3$ sample was prepared by adding an aqueous solution of $Ba(NO_3)_2$ to γ-Al_2O_3, dispersed in distilled water, under continuous stirring. The pH was adjusted to 11.0 by addition of NH_4OH and the slurry was further stirred for 20 min and then freezed with liquid nitrogen, freeze-dried and calcined in air at 600 °C for 1 h. In order to transform the precipitated BaO on alumina to $BaCO_3$, an aqueous solution of ammonium carbamate (NH_3NH_2COOH) was added to the BaO/Al_2O_3 powder under continuous stirring. The slurry was finally freezed, freeze-dried and calcined at 500 °C for 1 h.

Two $BaCO_3/Al_2O_3$ samples were prepared according to the procedure described above. The first one was prepared from γ-Al_2O_3 with a particle diameter (d) ≤ 10 μm, which was obtained by sieving of the γ-Al_2O_3 powder; while for the other sample, alumina with the original particle size distribution ($d \leq 150$ μm) was used. Further, two BaO loadings were chosen. The two $BaCO_3/Al_2O_3$ samples will be noted as 13% BaO/Al_2O_3(S) and 18% BaO/Al_2O_3(L) where 13 and 18% stands for the barium oxide content, (S) and (L) for small and large support particles, respectively.

2.1.2. Monolith samples for catalytic evaluation

Four cordierite monoliths (400 cells per square inch) with a length of 15 mm containing 188 channels were washcoated

Table 1
Sample washcoat compositions, BET surface area and platinum dispersion

Catalyst	Pt-precursor	Al_2O_3 (mg)	BaO (mg)	Pt (%)	BET (m^2)	Pt dispersion (%)
Cat. 1	H_2PtCl_6	588	126	1.8	83	3
Cat. 2	$Pt(NH_3)_4(OH)_2$	586	125	2.0	87	9
Cat. 3	$Pt(NH_3)_2(NO)_2$	597	121	2.1	75	2
Cat. 4	$Pt(NO_3)_2$	581	135	2.0	96	16

with alumina, impregnated with $Ba(NO_3)_2$ and, finally, impregnated with platinum. Four different platinum precursors were used in the preparation (one for each sample). The preparation method is described in detail in [26]. Briefly, the monoliths were coated with alumina by immersing the monolith in alumina slurry, blowing away excess slurry from the channels, drying in air at 95 °C for few seconds and calcining in air at 500 °C for 2 min. This procedure was repeated until the desired amount of alumina was obtained. Thereafter, the samples were calcined at 600 °C for 2 h. The same impregnation and drying procedure was used for impregnating the alumina coated samples with an aqueous solution of $Ba(NO_3)_2$. Thereafter, the samples were calcined at 600 °C for 2 h. In order to avoid dissolution of BaO during the impregnation with the platinum solutions, BaO was converted to $BaCO_3$ which is considerably less soluble in aqueous solutions than BaO. The transformation of BaO to $BaCO_3$ was performed by exposing the BaO/Al_2O_3 samples to air in closed sample holders. After 1 week, the samples were immersed in a solution of ammonium carbamate for 20 min, dried in air at 130 °C and calcined in air at 500 °C for 3 min. Before impregnation with platinum solution, the samples were washed in distilled water. The platinum impregnation was performed by filling the channels with the desired amount of platinum, diluted in distilled water. The samples were then dried in air at 80 °C for 12 h, calcined at 500 °C for 2 h and finally reduced in 2% H_2 in Ar at 500 °C for 1 h. The platinum precursor used for the first sample (Cat. 1) was hexachloroplatinic acid [$H_2Pt(Cl)_6$], while tetraammineplatinum hydroxide [$Pt(NH_3)_4(OH)_2$], diammineplatinum nitrite [$Pt(NH_3)_2(NO_2)_2$] and platinum nitrate [$Pt(NO_3)_2$] were used to prepare Cat. 2, Cat. 3 and Cat. 4, respectively. The quantities of the different washcoat components for all samples are given in Table 1.

2.2. Zeta potential measurements

The zeta potential of the Al_2O_3, $BaCO_3$ and $BaCO_3/Al_2O_3$ samples dispersed in water was measured as a function of pH using AcoustoSizer (Colloidal Dynamics, Warwick, RI) at frequencies between 0.3 and 11 MHz. The device is supplied with a cell into which the sample suspension is poured. The cell contains a stirrer and three probes for pH, temperature and conductivity measurements. Automatic titration over desired pH ranges can be performed due to the built-in syringe pumps for the acid and base containers which are controlled by the computer software.

Prior to each measurement, the pH probe, air and standard solution (KSiW) calibrations were performed. The last two calibrations are necessary for accurate determination of an instrumental factor (*A*).

The samples were prepared by slowly adding 3.5 g sample to 350 ml distilled water and the suspension was continuously stirred for 3 h before performing the measurement. Some of the samples were also stabilized by adding 0.085 g $NaNO_3$ to the suspension and deagglomerated by using a high-energy ultrasonic probe. The measurements were conducted at room temperature and started after programming an automatic titration with 10-min delay for each pH step in order to allow the suspension to equilibrate. The pH of the samples was increased by adding NaOH.

2.3. FTIR measurements

In situ FTIR measurements were performed for the Al_2O_3, $BaCO_3$ and $BaCO_3/Al_2O_3$ samples in diffuse reflectance (DRIFT) mode with a Bio-Rad FTS6000 spectrometer equipped with a Harrick Praying Mantis DRIFT cell. Prior to each measurement, the powder sample was pretreated at 400 °C in Ar for 15 min, cooled to 30 °C in Ar and a background spectrum was taken followed by an immediate sample scan and another scan after 10 min. The sample was then exposed to CO_2 (100%) for 30 min and during this time several sample scans were collected. After the CO_2 exposure, the sample was flushed with Ar for 10 min and a new sample scan was taken. Finally, the sample was heated in Ar to 120 °C for 5 min to desorb the weakly adsorbed CO_2 and cooled down to 30 °C and the final spectrum was taken.

2.4. XRD measurement

An X-ray diffractogram was recorded for the $BaCO_3/Al_2O_3$ sample with a Siemens D500 X-ray powder diffractometer supplied with Göbel mirror system using Cu Kα radiation in order to verify the transformation of BaO to $BaCO_3$.

2.5. Catalyst characterization

The platinum dispersion of the catalysts was determined using N_2O dissociation, where for each dissociated N_2O molecule one gaseous N_2 molecule is formed and one oxygen atom is left on each surface platinum atom according to the following reaction [27]:

$$Pt_s + N_2O_{(g)} \rightarrow Pt{-}O + N_{2(g)}$$

where Pt_s denotes a surface platinum atom. The experiments were conducted in a flow reactor with a quartz tube in which the catalyst was placed. A thermocouple used to control the

temperature was placed 10 mm in front of the catalyst. Another thermocouple was placed inside the catalyst to measure the catalyst temperature. A mass spectrometer (Balzer QME 120) was connected to the reactor to analyse the outflow gas composition. The gas flow into the reactor was controlled with mass flow controllers. More details about this reactor are found in [28].

Prior to each measurement, the catalyst was first pre-oxidized for 10 min in 2% O_2 in Ar, flushed with Ar for 5 min, pre-reduced in 4% H_2 in Ar and flushed with Ar for 10 min at 500 °C. The temperature was then decreased to 90 °C and the catalyst was instantly exposed to 500 ppm N_2O in Ar for 20 min. The platinum dispersion was determined by integrating the N_2 (mass 28) signal during the N_2O exposure step after subtracting the amount of N_2 which originates from the cracking of N_2O in the mass spectrometer. The number of formed N_2 molecules is considered to be equal to the number of available platinum atoms on the sample surface [27]. Fig. 1a displays the N_2O, N_2 and O_2 signals from the mass spectrometer as a function of time during N_2O dissociation experiment performed for Cat. 4 (shown as an example), while Fig. 1b, shows the amount of gaseous N_2 which corresponds to the dissociation of N_2O as a function of time for all four samples.

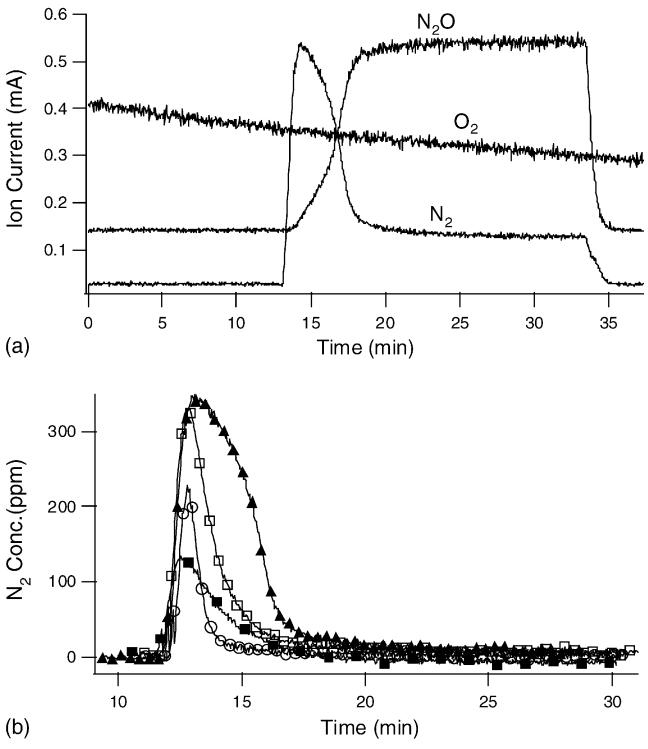

Fig. 1. N_2O dissociation experiments performed by exposing the catalysts to 500 ppm N_2O in Ar at 90 °C. Total flow = 200 ml/min. (a) Mass spectrometer signals as a function of time during a N_2O dissociation experiment performed on Cat. 4 (prepared from platinum nitrate). (b) The formation of N_2 (in ppm) as a function of time during the N_2O dissociation step for all four catalysts. Catalysts: Cat. 1 (◯), Cat. 2 (□), Cat. 3 (■) and Cat. 4 (▲).

The specific surface area of the catalysts was determined by nitrogen adsorption according to the BET method using a Digisorb 2600 (Micromertics) instrument. The platinum dispersion and the specific surface area of the catalysts are given in Table 1.

2.6. Activity measurements

The activity of the catalysts for continuous and transient NO_x reduction and NO_2 dissociation was tested in a flow reactor with a quartz tube in which the catalyst was placed. This reactor is described in detail in [26]. A thermocouple used to control the temperature was placed 10 mm in front of the catalyst. Another thermocouple was placed inside the catalyst to measure the catalyst temperature. A chemiluminescense detector (CLD 700) was connected to the reactor to monitor the NO_x, NO and NO_2 concentrations, while CO_2 was measured by a non-dispersive IR Maihak UNOR 610 instrument. The inlet gas composition was controlled by an Environics 2000 gas mixer. The gas flow and space velocity in all experiments were 3000 ml/min and 38,000 h^{-1}, respectively, with Ar as the carrier gas.

2.6.1. Heating ramp experiments

Prior to the heating ramp experiments, the catalysts were reduced in 2% H_2 at 500 °C for 30 min, flushed with Ar for 5 min and finally oxidized in 8% O_2 for 15 min. After the pre-treatment, the samples were cooled down to room temperature in Ar. The catalysts were then exposed to a reaction gas mixture of 400 ppm NO, 650 ppm C_3H_6 and 8% O_2 in Ar for 1 h at room temperature. The temperature was finally linearly increased with 5 °C/min to 450 °C.

2.6.2. Transient experiments

Prior to the transient experiments, the catalysts were pre-treated at 500 °C by reduction in 2% H_2 for 20 min, flushing with Ar and oxidation in 8% O_2 for 15 min. The catalysts were then cooled in Ar to 300 °C, stabilized in a lean gas mixture consisting of 400 ppm NO, 650 ppm C_3H_6 and 8% O_2 in Ar for 40 min and regenerated in a rich gas mixture for 4 min by switching of the oxygen supply and compensating that with Ar in order to maintain the total flow constant. Five lean/rich cycles were performed with 16 and 4 min long lean and rich periods, respectively.

2.6.3. NO_2 dissociation

The decomposition of NO_2 over the catalysts was investigated at 350 °C. The experiments were performed after reducing the catalysts in 2% H_2 in Ar for 10 min at 500 °C and cooling down in Ar to 350 °C. The NO_2 dissociation experiments were performed by exposing the catalysts to 630 ppm NO_2 in Ar for 3 h.

A summary of the gas compositions for all reactor experiments are given in Table 2.

Table 2
Summary of gas compositions

Experiment	NO (vol. ppm)	NO_2 (vol. ppm)	O_2 (vol.%)	C_3H_6 (vol. ppm)	Ar
$NO/C_3H_6/O_2$ heating ramp	400	–	8.0	650	Balance
NO_x storage reduction/lean condition	400	–	8.0	650	Balance
NO_x storage reduction/rich condition	400	–	–	650	Balance
NO_2 dissociation	–	630	–	–	Balance

3. Results and discussion

3.1. Surface characterization

The impregnation of the catalyst support with precious metals is crucial for the catalytic performance, since the interaction between the precious metal and the components of the support material can play an important role in dispersing the precious metal on the surface. In the case of NO_x storage, it has been concluded that both the storage and reduction of NO_x proceed via spill-over of intermediates between the precious metal and the storage sites [11]. This means that the interface between the storage material and the precious metal sites is crucial in the storage and reduction mechanisms. An investigation of the composition and properties of the surface on which the active material is deposited can facilitate the interpretation of the experimental results. For this reason we have performed the following surface characterization measurements described in the following sections.

3.1.1. Zeta potential measurements

As mentioned in Section 2, alumina with two different particle size distributions was used in this study. The aim was to prepare two different $BaCO_3/Al_2O_3$ samples, one with a low amount $BaCO_3$ precipitated on Al_2O_3 (S, i.e. $d \leq 10\,\mu m$) and the other with a higher amount $BaCO_3$ precipitated on Al_2O_3 (L, i.e. $d \leq 150\,\mu m$). Fig. 2a displays the results from zeta potential measurements performed using Al_2O_3(S), 13% BaO/Al_2O_3(S) and $BaCO_3$ suspensions. All three samples were provided with $NaNO_3$ and deagglomerated in a high-energy ultrasonic probe for 20 min. As shown in the figure, the point of zero charge (PZC) for Al_2O_3(S) is at pH ∼9.1, for $BaCO_3$ at pH ∼12.8 and for 13% BaO/Al_2O_3(S) at pH ∼10.5. Fig. 2b displays the same kind of measurements performed using Al_2O_3(L), $BaCO_3$ and 18% BaO/Al_2O_3(L) slurries. These measurements were performed without deagglomeration and $NaNO_3$ addition. As shown in the figure, the PZC for Al_2O_3(L) occurs at pH ∼8.1, for $BaCO_3$ at pH ∼12.8 and for 18% BaO/Al_2O_3(L) at pH ∼12.1.

It is important to mention that the values of the zeta potential as a function of pH for a particular material depend on many parameters, e.g. whether the material is solid or porous, the electrolyte concentration, the presence of impurities or additives, and the measurement method. In general, it is expected that the zeta potential at the extreme pH values should be considerably higher than at pH ranges close to the PZC. This may depend on a partial dissolution of the material and/or an increase in the electrolyte concentration during the titration to higher or lower pH values. The pH values for all sample suspensions before starting the titration were >7. In this study the measured Smolochofsky zeta potential values for the Al_2O_3 and $BaCO_3$ samples are generally lower than what is reported in the literature. In the case of γ-Al_2O_3, which is highly porous, this does not necessarily mean that our samples are low-charged. It is rather a consequence of the zeta potential and particle size distribution calculation algorithm in the AcoustoSizer software which assumes solid particles. According to O'Brien [29] more accurate zeta potential values and particle size distributions can be obtained for porous systems by modifying the calculation algorithms. We have, however, not performed any corrections of the calculation procedure since our main interest is to determine the PZC for each sample. The PZC for porous systems does not differ significantly from the corresponding solid systems since all particles with zero charge are immobile in the applied electric field. The PZC for the Al_2O_3 samples (at pH 8–9) is in good agreement with the literature. Concerning the PZC for the $BaCO_3$ samples, we observe some discrepancy

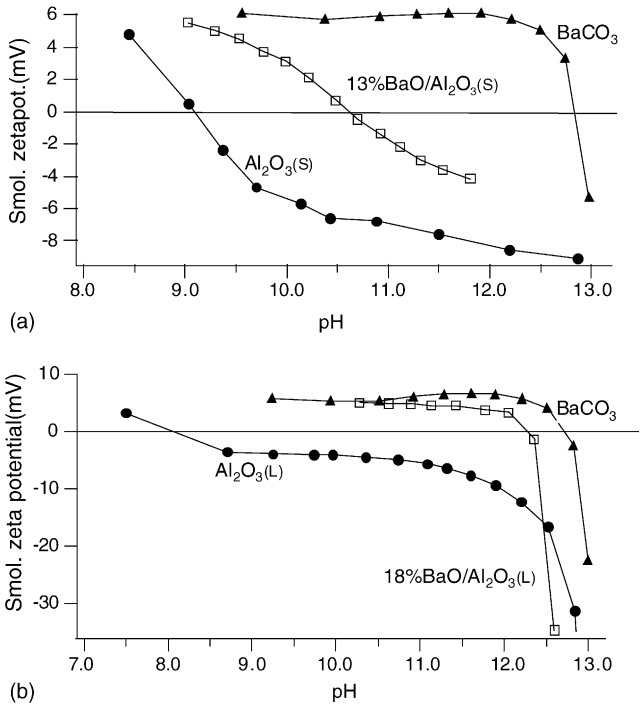

Fig. 2. Measured Smolochofsky zeta potential as a function of pH for: (a) deagglomerated Al_2O_3 ($d \leq 10\,\mu m$), $BaCO_3$ and 13% BaO/Al_2O_3 ($d \leq 10\,\mu m$) slurries and (b) Al_2O_3 ($d \leq 150\,\mu m$), $BaCO_3$ and 18% BaO/Al_2O_3 ($d \leq 150\,\mu m$) slurries.

with the corresponding values reported by Li and Jean [30], who report a PZC for $BaCO_3$ at pH around 10.5. However, we believe that this discrepancy may depend on differences in the preparation of the sample suspensions and purity of the $BaCO_3$ used in the investigations.

The most interesting feature in the results of these experiments is the PZC for the $BaCO_3/Al_2O_3$ samples. As it is seen in Fig. 2, the PZC values for both the higher and lower Ba-loaded sample is in between the corresponding values for pure Al_2O_3 and pure $BaCO_3$. Further, when the barium content increases, the PZC of the sample approaches the corresponding value for pure $BaCO_3$. This is clear from the difference between the PZC for the two $BaCO_3/Al_2O_3$ samples. The first sample, 13% BaO/Al_2O_3(S) with low amount of $BaCO_3$ precipitated on small Al_2O_3 particles has a PZC more close to the corresponding value for Al_2O_3 than for $BaCO_3$, while the 18% BaO/Al_2O_3(L) with higher amount $BaCO_3$ precipitated on larger Al_2O_3 particles has a PZC value more close to $BaCO_3$ than Al_2O_3. Although the results from these experiments are not sufficient to describe the surface composition, they indicate the changes in the surface charge properties when the $BaCO_3$ concentration in the samples is varied.

3.1.2. FTIR measurements

FTIR measurements were performed in order to verify the results from zeta potential measurements, which indicated that the Al_2O_3 surfaces in the $BaCO_3/Al_2O_3$ samples were not completely covered with $BaCO_3$. Labalme et al. [31] performed FTIR measurements to investigate the basic properties of the support (alumina) of Pt/Al_2O_3 and $Pt/BaO/Al_2O_3$ catalysts by CO_2 adsorption. The authors observed formation of HCO_3^- upon the adsorption of CO_2 on surface hydroxyl groups of alumina. The vibration bands assigned to HCO_3^- were located at 1644, 1490, 1450 and 1235 cm^{-1}. An earlier IR study based on CO_2 adsorption on alumina was performed by Parkyns and Road [32], where the authors assigned the vibrations at 3605 cm^{-1} (ν_{OH}), 1640 cm^{-1}(asym. ν_{CO}), 1480 cm^{-1} (sym. ν_{CO}) and 1233 cm^{-1} (ν_{C-OH}) to HCO_3^- formation as well. In Fig. 3 we show our results from similar measurements, i.e., CO_2 adsorption, performed on Al_2O_3(S), 13% BCO/Al_2O_3(S), 18% BaO/Al_2O_3(L) and $BaCO_3$. The FTIR spectra are recorded after exposing the samples to CO_2 for 30 min, flushing with Ar for 10 min, removing the weakly adsorbed CO_2 by heating the samples to 120 °C and cooling to 30 °C. Interestingly, the pure $BaCO_3$ sample did not show any interaction with the exposed CO_2. However, the Al_2O_3 and both $BaCO_3/Al_2O_3$ samples have coincident bands at 1658, 1437, 1229 and 3625 cm^{-1} which are assigned to the formation of HCO_3^- on alumina OH-groups. For the $BaCO_3/Al_2O_3$ samples, three additional bands at 1340, 1360 and 1530 cm^{-1} are observed. Those bands can be assigned to barium carbonate, where according to Mahzoul et al. [7], barium carbonate has a broad band centered at 1455 cm^{-1} with shoulders at 1316 and 1561 cm^{-1}. The barium carbonate is possibly formed by the interaction of CO_2 with BaO spots which were not transformed to $BaCO_3$ during the preparation of $BaCO_3/Al_2O_3$ samples.

The results from the FTIR study indicate that both $BaCO_3$ and Al_2O_3 domains are present on the surface of $BaCO_3/Al_2O_3$ samples. This is seen from the formation of HCO_3^- species on the Al_2O_3 and the $BaCO_3/Al_2O_3$ samples and the negative peaks at 3767 cm^{-1} which appears as the OH-groups of alumina is consumed in the formation of HCO_3^- species.

3.2. Reactor measurements

3.2.1. Heating ramp experiments with lean gas mixture

The outlet concentrations of NO, NO_2, NO_x and CO_2 as a function of catalyst temperature during heating ramp experiments performed using the samples with hexachloroplatinic acid (Cat. 1), tetraammineplatinum hydroxide (Cat. 2), diammineplatinum nitrite (Cat. 3) and platinum nitrate (Cat. 4) as the Pt-precursor are shown in Fig. 4 (a, b, c and d, respectively). For all catalysts, as soon as the temperature ramp starts, the NO_x signal increases and exceeds the inlet NO_x concentration, due to the desorption of weakly adsorbed NO_x species at room temperature. The NO_x concentrations reach maximum values at ~150 °C and, thereafter, start to decrease to reach minimum values in the temperature interval

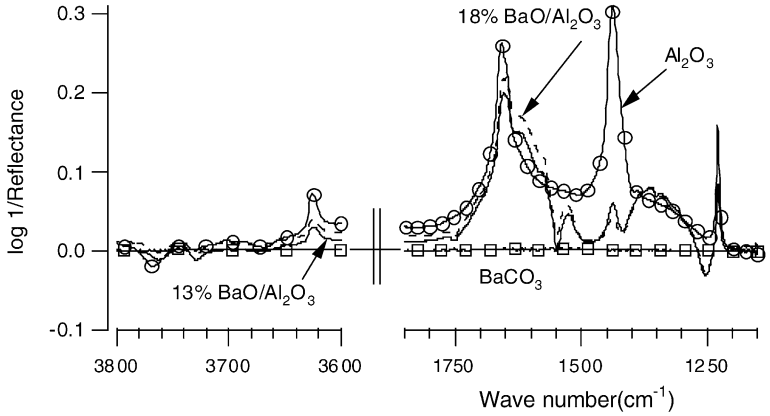

Fig. 3. FTIR spectrum of CO_2 adsorbed at 30 °C on Al_2O_3 (◯), $BaCO_3$ (□), 13% BaO/Al_2O_3 (···) and 18% BaO/Al_2O_3 (—) powder samples.

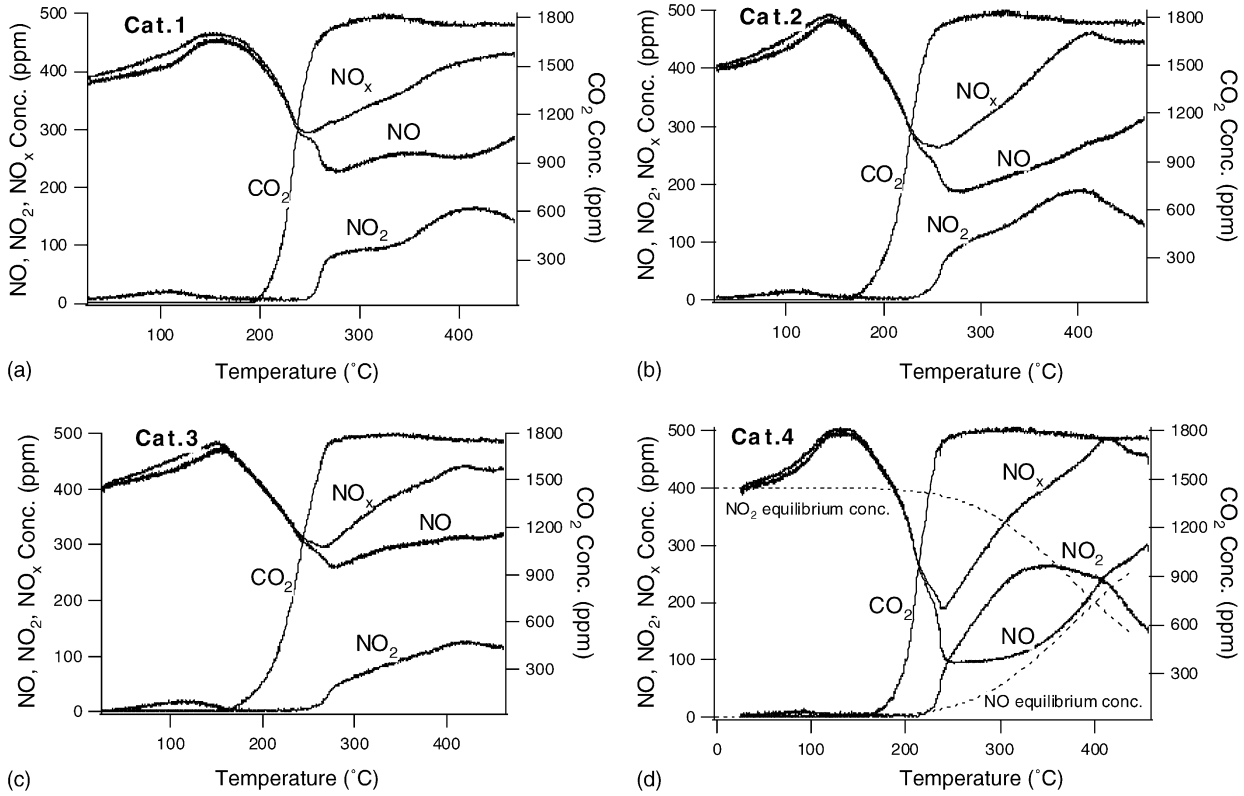

Fig. 4. Outlet concentration of NO, NO_2, NO_x and CO_2 as a function of temperature from $NO/C_3H_6/O_2$ heating ramp experiments conducted on: (a) Cat. 1 (prepared using hexachloroplatinic acid), (b) Cat. 2 (prepared using tetraammineplatinum hydroxide), (c) Cat. 3 (prepared using diammineplatinum nitrite) and (d) Cat. 4 (prepared using platinum nitrate). Gases: 400 vol. ppm NO, 650 vol. ppm C_3H_6 and 8 vol.% O_2 in Ar. Total flow = 3000 ml/min.

240–270 °C. The decrease in NO_x concentration is due to NO_x reduction by C_3H_6, which is also seen from the increase in the CO_2 signal. After a further temperature increase, both NO_2 and NO_x signals increase. This indicates that parallel oxidation and reduction processes of NO_x take place up to a certain temperature. As the temperature is further increased, the NO_2 formation increases while the NO_x reduction decreases. From the measured NO, NO_2 and N_2O signals from a similar experiment with NO, O_2 and C_3H_6 over a $Pt/BaO/Al_2O_3$ sample, Salasc et al. [33] showed that when the NO_2 signal reaches a maximum value, both the measured N_2O and the calculated N_2 signals reach zero.

From Fig. 4, it is clear that the NO oxidation only reaches equilibrium for Cat. 4, where NO and NO_2 have the same concentration at 407 °C. According to the thermodynamics, this should occur at 400 °C. However, due to the exothermic C_3H_6 oxidation, the catalysts temperature was slightly higher than the gas phase temperature. For comparison, the calculated equilibrium concentrations for NO and NO_2 are shown in Fig. 4d. It is worth to mention that the higher total NO_x concentrations in comparison to the calculated equilibrium NO and NO_2 concentrations at temperatures >360 °C are related to the release of stored NO_x as nitrate.

When considering the conversion of C_3H_6, the light-off temperatures (i.e. 50% conversion) for the four catalysts occur in the range 210–240 °C with the lowest temperature value shown by (Cat. 4), followed by (Cat. 2), (Cat. 1) and (Cat. 3), respectively.

To compare the oxidation and reduction activities, the NO_2 and NO_x traces from all samples are plotted as a function of temperature and shown in Fig. 5. As it is clear from the figure, Cat. 4 is the most active catalyst. This is seen from the

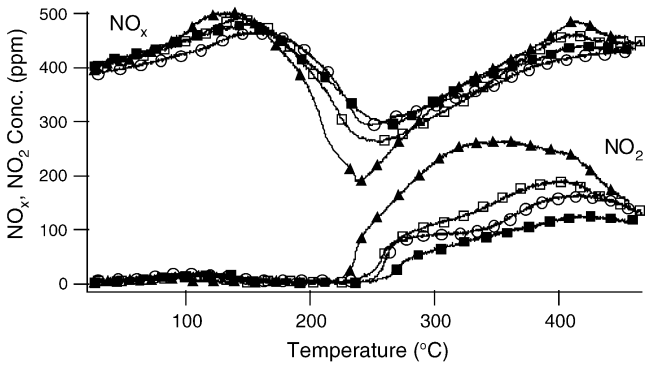

Fig. 5. Outlet concentration of NO_2 and NO_x as a function of temperature from $NO/C_3H_6/O_2$ heating ramp experiments conducted on Cat. 1 (prepared using hexachloroplatinic acid), Cat. 2 (prepared using tetraammineplatinum hydroxide), Cat. 3 (prepared using diammineplatinum nitrite) and Cat. 4 (prepared using platinum nitrate). Gases: 400 vol. ppm NO, 650 vol. ppm C_3H_6 and 8 vol.% O_2 in Ar. Total flow = 3000 ml/min. Catalysts: Cat. 1 (◯), Cat. 2 (□), Cat. 3 (■) and Cat. 4 (▲).

lowest NO_x minimum value due to highest reduction activity and highest NO_2 signal due to highest oxidation activity in comparison with the other catalysts. Next in activity is Cat. 2 followed by Cat. 1 and finally Cat. 3. The enhanced activity for oxidation and reduction for Cat. 4 in comparison with the other catalysts can possibly be related to a higher amount of accessible active sites for reaction and larger interface between the active sites and the support compounds.

3.2.2. Transient NO_x storage experiments

The capacity for NO_x storage and activity for NO_x reduction were investigated by performing transient lean/rich cycle experiments. For each sample five such cycles were performed in order to verify the reproducibility of the capacity for storage and activity for reduction. In Fig. 6, the outlet NO_x concentrations during such transients are shown for all catalysts. For clarity, only one cycle is shown (the third one) in the figure. As it is typical for NO_x storage during lean conditions, the NO_x signal increases with time until it reaches a steady state level after a certain time. A slow increase in the NO_x signal indicates a higher storage capacity. Another often observed feature is the breakthrough peak from desorbing NO when switching from lean to rich conditions. As it is obvious from the figure, the higher storage capacity is shown by Cat. 4, where the initial increase in NO_x signal is the slowest. Further, the NO_x concentration almost reaches zero during the rich conditions, which indicates a high activity for reduction for this catalyst. Next in storage capacity and activity for reduction is Cat. 2 followed by Cat. 1 and finally Cat. 3. Also in this case, the higher storage capacity and reduction activity for Cat. 4 may be related to the higher amount of active sites on the catalyst surface where more active sites take part in the oxidation and reduction processes. A summary over the performances for storage, reduction and oxidation for all catalysts is found in Table 3. The NO_x storage capacity is displayed as moles stored NO_x per moles barium during one lean period. The reduction activity is displayed by calculating the ratio of the integrated outlet to inlet NO_x concentrations during one rich period. The reduction of the stored NO_x is not included in the calculation. We assume a complete reduction of the stored NO_x since the storage capacity was reproducible for all catalysts. Finally, the NO_2 formation is obtained by calculating the ratio of the integrated outlet NO_2 to inlet NO signals during one lean period.

Table 3
NO_x storage capacity and activity for NO_x reduction and NO_2 formation during transient lean/rich experiments

Catalyst	NO_x storage (mol NO_x/mol BaO)	NO_x reduction (%)	NO_2 formation (%)
Cat. 1	0.15	78	35
Cat. 2	0.20	86	39
Cat. 3	0.10	66	24
Cat. 4	0.24	91	54

3.2.3. NO_2 dissociation

In the final flow-reactor experiment, the activity for NO_2 dissociation was studied. The aim with these experiments was to study the stability of the active sites against oxidation since NO_2 is a strong oxidation agent [12]. Fig. 7 displays the outlet concentrations of NO_x and NO as a function of time resulting from exposing the catalysts to 630 ppm NO_2 in Ar at 350 °C. The first 10 min of the experiment indicate some NO_x storage where the NO_x signal rises up to a constant concentration during the rest of the experiment.

Even in this experiment, Cat. 4 is the most active catalyst, where it shows the highest activity for NO_2 dissociation (highest outlet NO concentration) compared to the other catalysts and, further, a NO level that remains stable during the entire experiment. For the other three catalysts, the NO signal decreases with time. The most rapid decrease in NO signal occurs for Cat. 1 followed by Cat. 3. As it is clear from the figure, the NO outlet signal from these two catalysts is

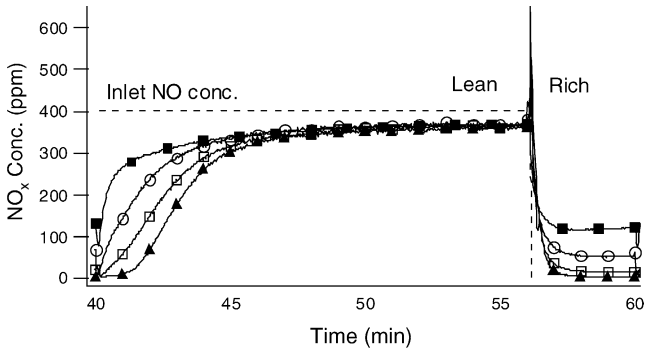

Fig. 6. Measured NO_x concentration as a function of time during one lean (16 min)/rich (4 min) cycle conducted at 300 °C. Catalysts: Cat. 1 (prepared using hexachloroplatinic acid), Cat. 2 (prepared using tetraammineplatinum hydroxide), Cat. 3 (prepared using diammineplatinum nitrite) and Cat. 4 (prepared using platinum nitrate). The gas composition during lean conditions was: 400 vol. ppm NO, 650 vol. ppm C_3H_6 and 8 vol.% O_2 and for rich condition, O_2 was switched off. Total flow = 3000 ml/min. Catalysts: Cat. 1 (◯), Cat. 2 (□), Cat. 3 (■) and Cat. 4 (▲).

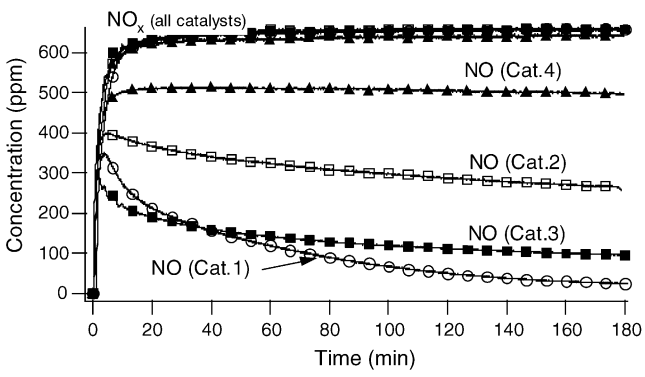

Fig. 7. NO and NO_x traces from NO_2 dissociation experiments conducted at 350 °C. Catalysts: Cat. 1 (prepared using hexachloroplatinic acid), Cat. 2 (prepared using tetraammineplatinum hydroxide), Cat. 3 (prepared using diammineplatinum nitrite) and Cat. 4 (prepared using platinum nitrate). Gases: 630 vol. ppm NO_2 in Ar. Total flow = 3000 ml/min. Catalysts: Cat. 1 (◯), Cat. 2 (□), Cat. 3 (■) and Cat. 4 (▲).

significantly lower than the corresponding signals from Cat. 2 and Cat. 4. The decrease in the NO concentration is connected to Pt deactivation with time due to Pt oxide formation [12]. It is worth to mention that this experiment was repeated for Cat. 4 with a reproducible result (not shown). This may indicate that the platinum in this sample is more resistant against oxidation compared to platinum in the other three samples.

3.3. The effect of the platinum precursor on the catalytic performance

The results from the reactor measurements show a clear difference in the catalytic activity between the four tested samples. Obviously, the activity of the catalyst prepared from platinum nitrate (Cat. 4) is significantly higher than for the other three catalysts in all activity measurements. The second most active catalyst is the catalyst prepared using tetraammineplatinum hydroxide (Cat. 2), which show a slightly higher activity in all measurements than the catalyst with hexachloroplatinic acid (Cat. 1) as Pt-precursor and the catalyst prepared using diammineplatinum nitrite (Cat. 3). Concerning the activity of the two last named catalysts, it is clear that Cat. 1 is more active than Cat. 3 both for continuous and transient NO_x reduction, but less active for NO_2 dissociation.

It is worth mentioning that all four samples have been prepared at the same time and, as shown in Table 1, the differences between the amounts of washcoat material for these samples are small and not significant. This means that the $BaCO_3/Al_2O_3$ surfaces for all four samples most likely had the same chemical properties before the impregnation with the platinum salt. Since solutions of different platinum salts were used for the impregnation of the active material, the difference in the catalytic performances can be related to the interaction of these different platinum solutions with the $BaCO_3/Al_2O_3$ surfaces.

According to Brunelle [14], the key parameters which control the interaction between the support surface and the Pt-precursor are: the PZC of the metal oxide, the pH of the aqueous solution and the nature of the metallic complex. In order to predict possible interaction mechanisms between the platinum and the support surface, data on the support surface polarization as a function of pH is required.

The surface polarization of the $BaCO_3/Al_2O_3$ coated monolith samples in contact with aqueous solutions is comparable with the 18% BaO/Al_2O_3 powder samples due to the almost equal amounts of barium loading. Taking into account the results from the zeta potential measurements, we can consider the $BaCO_3/Al_2O_3$ surface in contact with aqueous solutions to be positively charged at pH values <11, zero charged at pH 11–12 and negatively charged at pH values >12.

The interaction between the Pt-precursor solution and the support oxide surface can be interpreted with the help of the following mechanisms: (i) electrostatic interaction, (ii) ion-exchange, and (iii) ligand-exchange [13,14,16–20,22–24,34,35].

The interaction of the four Pt-precursors which are used in this work with the $BaCO_3/Al_2O_3$ surfaces will be discussed below from the point of view of the three mechanisms mentioned above.

3.3.1. Platinum nitrate–$BaCO_3/Al_2O_3$ interaction (Cat. 4)

The pH of the platinum nitrate solution prepared for Cat. 4 was ∼3. Since the $BaCO_3/Al_2O_3$ surface is positively charged at this pH value, electrostatic attraction takes place with negatively charged ions and complexes in the impregnation solution. However, according to Dou et al. [34], the Pt complexes in platinum nitrate solutions are positively charged at low pH values. This means that the electrostatic interaction under these conditions might be repulsive. Furthermore, Dou et al. [34] suggest that the Pt species interact with the support surface via ligand-exchange, where a labile terminal H_2O ligand is exchanged with a surface Al–OH group. The platinum nitrate adsorption on the support seems to be fast and completed in a few minutes, which results in Pt deposition on the outer surface of the support [34]. Another interesting feature, reported by Dou et al. [34], is the stability of positively charged oligomeric Pt complexes, in acidic solutions preventing agglomeration and precipitation.

From the discussion above, the high activity of the sample prepared by platinum nitrate may be related to the stability of Pt complexes which anchor preferably to Al_2O_3 than $BaCO_3$ particles via ligand-exchange. Since the adsorption of Pt is rapid, then, the subsequent drying process does not effect the Pt distribution on the surface significantly. Further, since the catalyst prepared by platinum nitrate showed high activity for NO_x reduction and high capacity for NO_x storage, we assume that the Pt particles are well distributed on the surface, with sufficiently large interface area with both Al_2O_3 and $BaCO_3$. Furthermore, the high stability of the Pt-particles against oxidation in this catalyst (Cat. 4) indicates that the Pt particles are preferably anchored close to Al_2O_3 rather than to $BaCO_3$ surface particles, since a close contact between platinum and barium may promote electronic interactions, which suppresses the catalytic activity [36].

3.3.2. Hexachloroplatinic acid–$BaCO_3/Al_2O_3$ interaction (Cat. 1)

In contrast to platinum nitrate, the hexachloroplatinic acid is well studied in the literature. The pH for the hexachloroplatinic acid solution used for the preparation of Cat. 1 was ∼3. Studies on the hexachloroplatinic acid speciation as a function of pH show that at pH value around 3, the impregnation solution is dominated by $[PtCl_6]^{2-}$ and $[PtCl_5(H_2O)]^{1-}$ complexes [25,17]. This means that for Cat. 1 the negatively charged platinum complexes may interact electrostatically with the positively charged $BaCO_3/Al_2O_3$ surface. Another suggested mechanism is interaction via ligand-exchange with the support surface. According to Shelimov et al. [13], an inner-sphere complex formation or grafting occurs upon impregnating alumina surfaces with hexachloroplatinic acid

solution. The ligand-exchange takes place, where the Al–OH surface groups replace some of the ligands of the $[PtCl_6]^{2-}$ complexes according to the following reactions [13]:

$$2Al\text{–}OH_{surface} + [PtCl_6]^{2-}_{solution} \leftrightarrow [(AlOH)_2PtCl_4]_{surface} + 2Cl^-_{solution} \quad (1)$$

and/or

$$2Al\text{–}OH_{surface} + [PtCl_6]^{2-}_{solution} \leftrightarrow [(AlCl)_2PtCl_4]_{surface} + 2OH^-_{solution} \quad (2)$$

The occurrence of these two reactions is possible in this study. This means that chlorines coordinating the Pt ions will remain on the surface after the impregnation. It is most likely that some chlorine traces are preserved on the surface of the catalyst after calcination and reduction with hydrogen, since we have not performed any special treatments to remove chlorine from the catalysts. Accordingly, the presence of chlorine traces may affect the catalytic properties negatively [37].

According to Dou et al. [34], complete adsorption of hexachloroplatinic acid seems not to occur, which is the case for platinum nitrate, even an hour after performing the Pt impregnation. This may also contribute to the lower catalytic activity, which was shown by Cat. 1 in comparison to Cat. 4.

It has also been reported that the pH value of the hexachloroplatinic acid solution can increase drastically upon impregnation with high surface area metal oxides [25]. This is due to the strong buffering effects of these oxides, since large concentrations of protons are consumed by the surface hydroxyl groups of the metal oxides [25]. An increased pH value of the precursor solution leads to an increase in the concentration of the uncharged complex $[PtCl_4(H_2O)_2]^0$, which interacts weakly with the surface. Uncharged complexes can easily migrate towards the catalyst exterior during the drying process [38].

3.3.3. Tetraammineplatinum hydroxide–$BaCO_3/Al_2O_3$ interaction (Cat. 2)

The tetraammineplatinum hydroxide solution used for the preparation of Cat. 2 was slightly basic with a pH value ~9. At this pH value, the $BaCO_3/Al_2O_3$ surface is still positively charged. From the literature, it seems that the dominating platinum complex in solutions of tetraammineplatinum hydroxide is $[Pt(NH_3)_4]^{2+}$ [14]. This indicates that for Cat. 2 the electrostatic interaction between the Pt complex and the surface is repulsive. However, according to Brunelle [14] and Goguet et al. [35], the $[Pt(NH_3)_4]^{2+}$ complex interacts with the support oxide via ion-exchange with protons on surface hydroxyl groups (of alumina or silica). This interaction seems to be strong, where the Pt complex remains on the surface during the drying process. During the calcination, the ammine groups decompose resulting in Pt particles coordinated with surface oxygen on the support [18].

3.3.4. Diammineplatinum nitrite–$BaCO_3/Al_2O_3$ interaction (Cat. 3)

The diammineplatinum nitrite solution used for the preparation of Cat. 3 was strongly basic with pH ~11. At this pH value, the $BaCO_3/Al_2O_3$ surface is very weakly or zero charged. This means that neither the electrostatic interaction, nor the ion-exchange mechanisms are favored during the Pt impregnation. It is probable that platinum forms an ammine complex as $[Pt(NH_3)]^{2+}$. However, the interaction between such complexes and the weakly charged or uncharged surface results in the migration of the complex to the exterior of the monolith during the drying process, which may explain the low reactivity of this catalyst.

4. Conclusions

In this work we have studied the effect of the interaction between platinum and the $BaCO_3/Al_2O_3$ surface on the catalytic activity. Since this interaction starts already when the washcoat is provided with the platinum precursor, we have also studied the surface charge of Al_2O_3, $BaCO_3$ and $BaCO_3/Al_2O_3$ powder samples as a function of pH by mean of zeta potential measurements. For the impregnation with Pt, we have used four different platinum precursors (two forming negatively charged platinum complexes and two forming positively charged Pt complexes). Furthermore, we have studied the surface composition of the $BaCO_3/Al_2O_3$ samples using FTIR spectroscopy.

From the results of the characterization measurements we can conclude that up to 18% BaO content, the surface contains both Al_2O_3 and $BaCO_3$ domains.

The catalytic activity measurements show that the catalyst prepared by platinum nitrate shows the highest activity for continuous lean NO_x reduction, NO_x storage and reduction, and NO_2 dissociation. Next in activity is the catalyst prepared from tetraammineplatinum hydroxide. The catalyst prepared from hexachloroplatinic acid is more active than the catalyst prepared from diammineplatinum nitrite for continuous NO_x reduction, NO_x storage and reduction, but less active in NO_2 dissociation.

From the platinum dispersion measurements and the catalytic activity measurements we find some correlations between the platinum dispersion and the catalytic activity where the catalyst with the highest dispersion shows the highest activity, due to highest accessible amount of Pt sites for reactions. The Pt dispersion is a function of the interaction between the Pt precursor and the $BaCO_3/Al_2O_3$ surface. Higher Pt dispersions can be achieved upon strong electrostatic attraction or ion and ligand-exchange between the Pt complexes and the surface.

Acknowledgments

This work has been performed within the Competence Centre for Catalysis, which is financially supported by the

Swedish National Energy Agency and the member companies: AB Volvo, Johnson Matthey-CSD, Saab Automobile Powertrain AB, Perstorp AB, AVL-MTC AB, Akzo Nobel Catalysts and The Swedish Space Corporation.

References

[1] S. Levitus, J.I. Antonov, J. Wang, T.L. Delworth, K.W. Dixon, A.J. Broccoli, Science 292 (5515) (2001) 267–270.
[2] E. Fridell, M. Skoglundh, S. Johansson, B. Westerberg, A. Törncrona, G. Smedler, Stud. Surf. Sci. Catal. 116 (1998) 537–547.
[3] E. Fridell, M. Skoglundh, B. Westerberg, S. Johansson, G. Smedler, J. Catal. 183 (2) (1999) 196–209.
[4] E. Fridell, H. Persson, B. Westerberg, L. Olsson, M. Skoglundh, Catal. Lett. 66 (1–2) (2000) 71–74.
[5] P. Engström, A. Amberntsson, M. Skoglundh, E. Fridell, G. Smedler, Appl. Catal. B: Environ. 22 (4) (1999) L241–L248.
[6] H. Mahzoul, J.F. Brilhac, P. Gilot, Appl. Catal. B: Environ. 20 (1) (1999) 47–55.
[7] H. Mahzoul, L. Limousy, J.F. Brilhac, P. Gilot, J. Anal. Appl. Pyrolysis 56 (2) (2000) 179–193.
[8] A. Amberntsson, M. Skoglundh, M. Jonsson, E. Fridell, Catal. Today 73 (3–4) (2002) 279–286.
[9] A. Amberntsson, M. Skoglundh, S. Ljungstrom, E. Fridell, J. Catal. 217 (2) (2003) 253–263.
[10] D. Uy, K.A. Wiegand, A.E. O'Neill, M.A. Dearth, W.H. Weber, J. Phys. Chem. B 106 (2) (2002) 387–394.
[11] L. Olsson, H. Persson, E. Fridell, M. Skoglundh, B. Andersson, J. Phys. Chem. B 105 (2001) 6895–6906.
[12] L. Olsson, E. Fridell, J. Catal. 210 (2) (2002) 340–353.
[13] B.N. Shelimov, J.-F. Lambert, M. Che, B. Didillon, J. Molec. Catal. A: Chem. 158 (1) (2000) 91–99.
[14] J.P. Brunelle, Pure Appl. Chem. 50 (9–10) (1978) 1211–1229.
[15] J.A. Schwarz, M.S. Heise, J. Colloid Interf. Sci. 135 (2) (1990) 461–467.
[16] B. Shelimov, J.F. Lambert, M. Che, B. Didillon, J. Catal. 185 (2) (1999) 462–478.
[17] J.R. Regalbuto, A. Navada, S. Shadid, M.L. Bricker, Q. Chen, J. Catal. 184 (2) (1999) 335–348.
[18] A. Munoz-Paez, D.C. Koningsberger, J. Phys. Chem. 99 (12) (1995) 4193–4204.
[19] V.M. Blachou, C.J. Philippopoulos, Chem. Eng. Commun. Int. J. Commun. Res. 119 (1993) 41–53.
[20] U. Olsbye, R. Wendelbo, D. Akporiaye, Appl. Catal. A: General 152 (1) (1997) 127–141.
[21] J.P. Bournonville, J.P. Franck, G. Martino, Stud. Surf. Sci. Catal. 16 (1983) 81–89.
[22] T. Mang, B. Breitscheidel, P. Polanek, H. Knozinger, Appl. Catal. A: General 106 (2) (1993) 239–258.
[23] R.D. Gonzalez, H. Miura, Catal. Rev.—Sci. Eng. 36 (1) (1994) 145–177.
[24] J.A.A. Van den Tillaart, J. Leyrer, S. Eckhoff, E.S. Lox, Appl. Catal. B: Environ. 10 (1–3) (1996) 53–68.
[25] W.A. Spieker, J. Liu, J.T. Miller, A.J. Kropf, J.R. Regalbuto, Appl. Catal. A: General 232 (1–2) (2002) 219–235.
[26] M. Skoglundh, H. Johansson, L. Lowendahl, K. Jansson, L. Dahl, B. Hirschauer, Appl. Catal. B: Environ. 7 (3–4) (1996) 299–319.
[27] M.H. Kim, J.R. Ebner, R.M. Friedman, M.A. Vannice, J. Catal. 204 (2) (2001) 348–357.
[28] P. Lööf, B. Kasemo, K.-E. Keck, J. Catal. 118 (1989) 339–348.
[29] R.W. O'Brien, J. Colloid Interf. Sci. 171 (2) (1995) 495–504.
[30] C.-C. Li, J.-H. Jean, J. Am. Ceram. Soc. 85 (12) (2002) 2977–2983.
[31] V. Labalme, N. Benhamou, N. Guilhaume, E. Garbowski, M. Primet, Appl. Catal. A: General 133 (2) (1995) 351–366.
[32] N.D. Parkyns, M. Road, J. Chem. Soc. (A) (1969) 410–417.
[33] S. Salasc, M. Skoglundh, E. Fridell, Appl. Catal. B: Environ. 36 (2) (2002) 145–160.
[34] D. Dou, D.-J. Liu, W.B. Williamson, K.C. Kharas, H.J. Robota, Appl. Catal. B: Environ. 30 (1–2) (2001) 11–24.
[35] A. Goguet, M. Aouine, F.J. Cadete Santos Aires, A. De Mallmann, D. Schweich, J.P. Candy, J. Catal. 209 (1) (2002) 135–144.
[36] G. Centi, G.E. Arena, S. Perathoner, J. Catal. 216 (1–2) (2003) 443–454.
[37] L. Van Tiep, M. Bureau-Tardy, G. Bugli, G. Djega-Mariadassou, M. Che, G.C. Bond, J. Catal. 99 (2) (1986) 449–460.
[38] T. Vergunst, F. Kapteijn, J.A. Moulijn, Appl. Catal. A: General 213 (2) (2001) 179–187.